A NEW TYPE OF LIMIT CYCLE OSCILLATION OCCURRED IN FLUTTER WING MODEL AT TRANSONIC WIND TUNNEL TESTS

Koji Miwa* and Jun Hatta*
***University of Fukui, Fukui, Japan**

Keywords: *Aeroelasticity, Transonic Flutter, Limit Cycle Oscillation, Subcritical Hopf Bifurcation*

Abstract

In the recent transonic wind tunnel tests for a high aspect ratio wing model, new types of limit cycle oscillation (LCO) were observed. When excitation was applied to the wing by activating a leading edge control surface, the forced oscillation of the wing was progressing into large amplitude LCO-like vibration, but when excitation was removed, the wing was getting out of the LCO state and stopped oscillation. Such behaviors were observed in this experiment for the first time. The present paper discusses the possibility that these new types of LCO occurred around a saddle-node bifurcation by performing a numerical simulation based on a nonlinear mathematical model characterizing transonic flutter.

1 Introduction

Flutter is a self-excited oscillation that can arise through the interactions of an aerodynamic flow with elastic modes of a mechanical structure such as bending-torsion coupling flutter for an aircraft wing. The occurrence of flutter leads to the destruction of an aircraft so that it is required for an aircraft not to encounter flutter until it reaches 15% higher speed than the maximally attainable speed.

In transonic region, flutter often takes the form of a limit cycle oscillation (LCO) caused by nonlinear behavior of transonic aerodynamics due to a shock wave moving on the wing surface coupled with the flow separation [1]-[3]. Also in this region, there is a phenomenon known as a transonic dip where the flutter velocity drops significantly against a flight Mach number [4].

A series of the wind tunnel tests for transonic flutter of a high aspect ratio wing model have been conducted at NAL (National Aerospace Laboratory, now Japan Aerospace Exploratory Agency (JAXA)) in Japan [5], and a nonlinear mathematical model that can explain the most of the bifurcation characteristics observed in the tests has been developed [6].

Bifurcation diagram of transonic flutter, either observed in the wind tunnel tests or predicted by the mathematical model, is classified as a subcritical Hopf bifurcation type, which means that the LCO type flutter may occur at lower dynamic pressure than the nominal flutter, by more than 10%.

In April 2005, we performed the new wind tunnel test at the transonic wind tunnel at JAXA for a week, and observed new type of LCO. In the previous tests, LCO once established due to disturbance was sustained with the same amplitude even after removed the disturbance. The new type of LCO observed in this test has the feature that it stopped oscillation as the disturbance was removed. It is first time in this test that we observed such phenomena. In this paper, this phenomenon is analyzed by performing a simulation for the nonlinear characteristics of the transonic flutter.

In the following, in Chapter 2 of this paper, we describe a high aspect ratio wing model and the typical transonic flutter. In Chapter 3, we describe new wind tunnel tests for transonic flutter and discuss the results. In Chapter 4, we describe the new type LCO. In Chapter 5, we describe the numerical simulation for new type LCO.

2 Wing model and its transonic flutter

2.1 High aspect ratio wing model and transonic wind tunnel

Figure 1 is a wing model used in transonic wind tunnel tests in JAXA. This wing model is a scale-down model of a civil aircraft's wing, which has a high aspect ratio. The wing model has a wing span of 1043 mm, a wing code of 369 mm at a wing root, 101 mm at a wing tip and a sweptback angle of 16.9 deg. In this wing model, a leading edge (l. e.) control surface was used in order to apply oscillatory disturbance to this wing model; a trailing edge (t. e.) control surface was used in active flutter control. In the present research t. e. control surface was not used. The two sets of motors driving leading and trailing edge control surfaces are installed at the enlarged center part of the wing. The wing has 7 sets of bending-torsion strain gages and 4 accelerometers for measuring a state of the wing. The wing has a line of 24 pressure holes along a wing chord and is used for static pressure measurement.

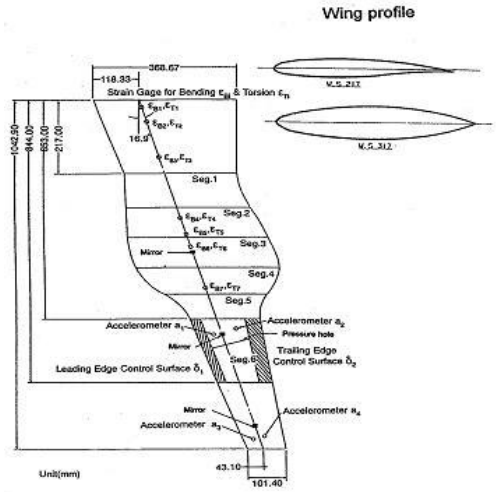

Fig. 1. High aspect ratio wing model

We used a transonic wind tunnel in JAXA. It is a closed-circuit facility, which has a 2×2 m^2 test section. The wing model is hung vertically from the ceiling of the wind tunnel test section (Fig. 2), with the incident at 0.75 deg. The wind tunnel has a flutter-stopping device. It eventually stops the flutter for protecting the wing model. A wind tunnel can change total pressure and Mach number.

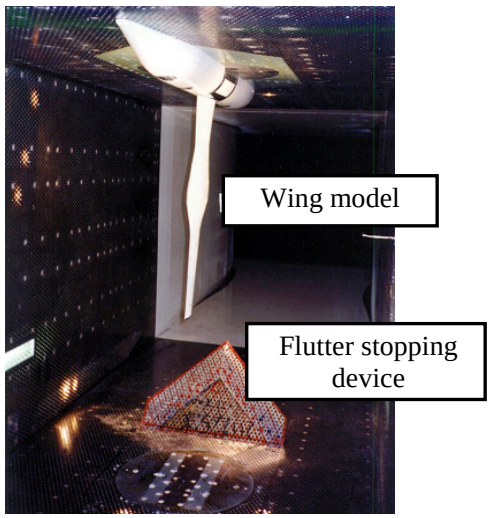

Fig. 2. Experimental set up

2.2 Typical transonic flutter

A typical result of the transonic wind tunnel tests for no-control is shown in Fig. 3. In this figure from the top chart to the bottom, an output of accelerometer, a deflection of a l. e. control surface and a dynamic pressure in the transonic wind tunnel are shown, respectively. As you can see at the top chart, LCO suddenly stops when the dynamic pressure goes down at a certain level.

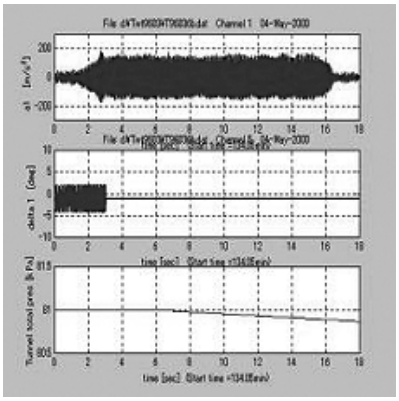

Fig. 3. Saddle-node bifurcation phenomenon due to quasi-static decrease of a wind tunnel dynamic pressure

Collecting all the experimental data obtained in transonic wind tunnel tests, we can get an experimental bifurcation diagram as shown in Fig. 4. A vertical axis expresses amplitude of LCO, and a horizontal axis expresses a dynamic pressure. Crosses in a figure express a stability boundary. When

excitation by vibrating the leading edge of the wing model is not enough to oscillate the wing model over the stability boundary, oscillation of a wing model stops as excitation is stopped. Conversely, when larger response occurs than a stability boundary, the wing model progresses to LCO and it is maintained, even if excitation is stopped. Circles express the amplitude of LCO.

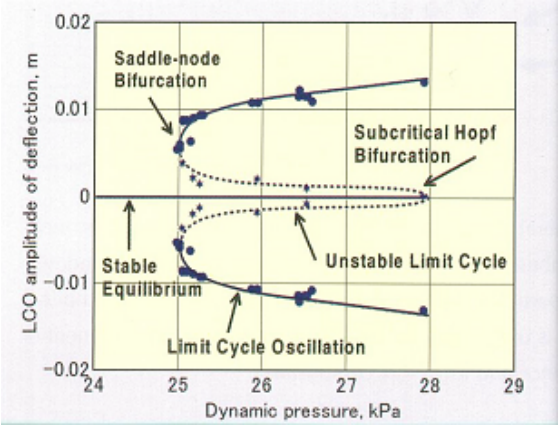

Fig. 4. Bifurcation diagram of experimental data

3 Transonic wind tunnel test

3.1 LCO test

The test aims at determining the stability boundary, i. e., unstable limit cycle at the bifurcation diagram in order to define the nonlinear phenomena of transonic flutter. Setting stepwise the amplitude of the leading edge control surface oscillation at a certain level, we search whether the wing model vibration goes to LCO or ceases to rest after removing the control surface oscillation.

The test was carried out as follows. After decreasing the wind tunnel total pressure to the proper value where flutter will not occur, we operated a fan to set test section Mach number at 0.80. We then increased the total pressure P_0 gradually until flutter occurs without exciting the wing. Measured value at flutter is defined as a critical flutter total pressure, P_f

We then kept the total pressure lower than the critical flutter value P_f, and investigated whether the wing model might come to LCO or not by oscillating the leading edge control surface. Testing total pressure was changed stepwise by 1 kPa. We first oscillated the leading edge surface with 1 deg, and increased until 5 deg. by 1 deg step if the wing did not come to LCO. In case the wing came to LCO, next step was reduced to half. Figure 5 shows the test procedure. When LCO doesn't occur at 2 deg and occurred at 3 deg, we proceed to 2.5 deg test next. The stability boundary can be obtained by this procedure. The minimum step of the control surface amplitude was 1.125 deg, though the value was changed as the total pressure since we decided the step size according to the wind conditions for safety reasons.

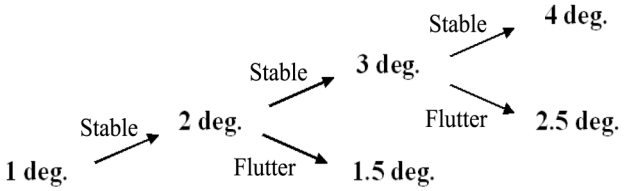

Fig. 5. Experimental procedure

Figure 6 shows the layout of the test set up. The strip-chart recorder and FFT analyzer are used for confirmation of the sensor outputs and for online prediction of the flutter occurrence. Each sensor output and control surface deflection data are recorded in the data recorder.

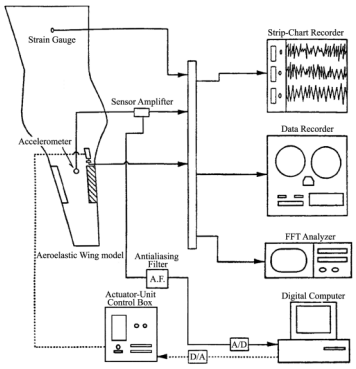

Fig. 6. Layout of experimental apparatus

3.2 Test results and discussion

Test results are shown in Fig. 7. Excitation amplitude of the l. e. surface in the vertical axis is depicted against the dynamic pressure of the wind tunnel test section in the horizontal axis. With Mach number M and total pressure P_0 of wind tunnel, dynamic pressure q can be expressed as the following equation.

$$q = \frac{1}{2}\rho u^2 = \frac{1}{2}\gamma \cdot P_0 \cdot M^2 \left(1 - \frac{\gamma - 1}{2} M^2\right)^{\frac{\gamma}{\gamma - 1}} \qquad (1)$$

The critical flutter total pressure P_f was 86.9 kPa (q = 25.5 kPa) in the first test, and LCO test was carried out in the range of total pressure 79 to 85 kPa. The critical pressure P_f changed to 85.5 kPa (q = 25.1 kPa) at the second test.

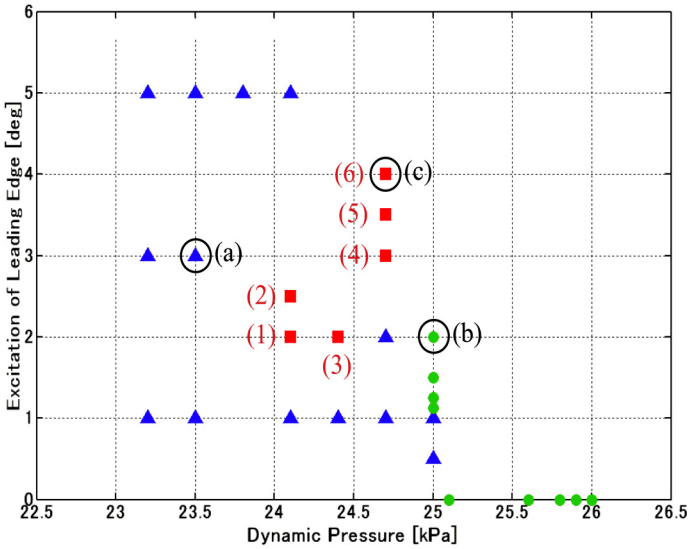

Fig. 7. Experimental results

The solid triangles in Fig. 7 show that the wing model was stable even applying excitation; the solid circles show that the wind model went to LCO in applying excitation. The solid squares, however, show that the wind model behaved as going to LCO in applying excitation, but it went down to equilibrium when removed excitation. The time history data for acceleration a_1 and leading edge control surface deflection δ_1 for each three cases are shown from (a) to (c) in Fig. 8. (a) shows data for total pressure P_0 = 85 kPa (q = 23.5 kPa) and excitation amplitude of l. e. surface 2.0 deg; (b) for P_0 = 85 kPa (q = 25.0 kPa) and l. e. surface 2.0 deg; (c) for P_0 = 84 kPa (q = 24.7 kPa) and = 4.0 deg. Because the flutter-stopping device was operated in (b), its operation is shown in the figure. The stopper was not used in (a) and (c).

As shown in Fig. 9 (a), the wing didn't go to large amplitude LCO by the l. e. surface excitation, but in Fig. 9 (b), the wing went to LCO even with smaller amplitude of excitation; LCO continued until the flutter stopping device was activated. However, in Fig. 9 (c), the same amplitude of LCO developed by the excitation was ceased to rest after stopping excitation.

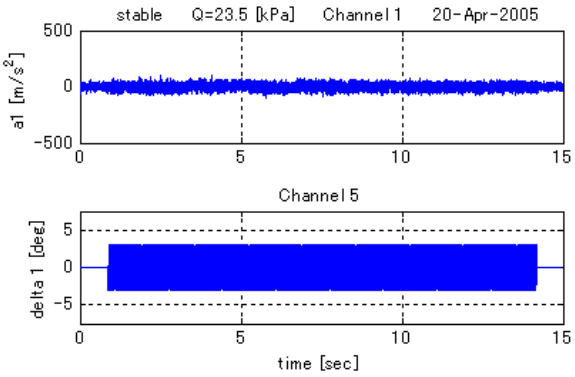

(a) Stable
q = 23.5 kPa, l.e. = 3.0 deg

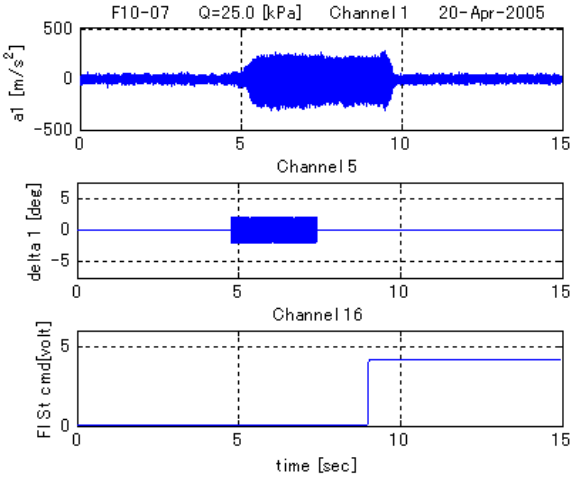

(b) LCO
q = 25.0 kPa, l.e. = 2.0 deg

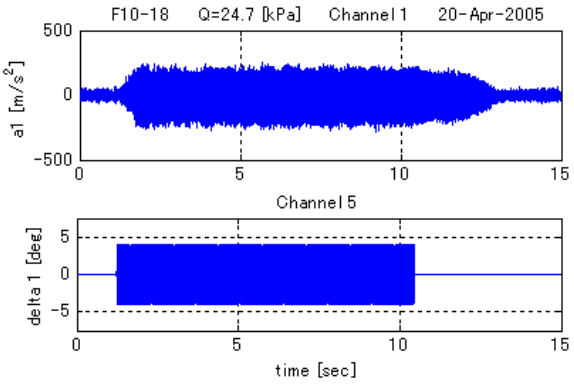

(c) LCO-Stable
q = 24.7 kPa, l.e. = 4.0 deg

Fig. 8. Time histories of experimental data

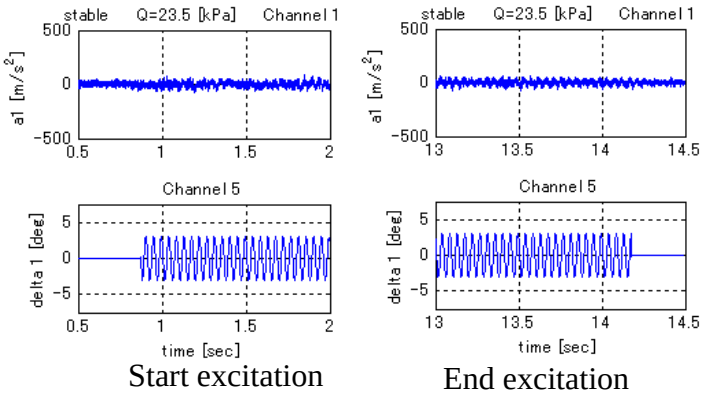

(a) Stable case (1.5 sec.)

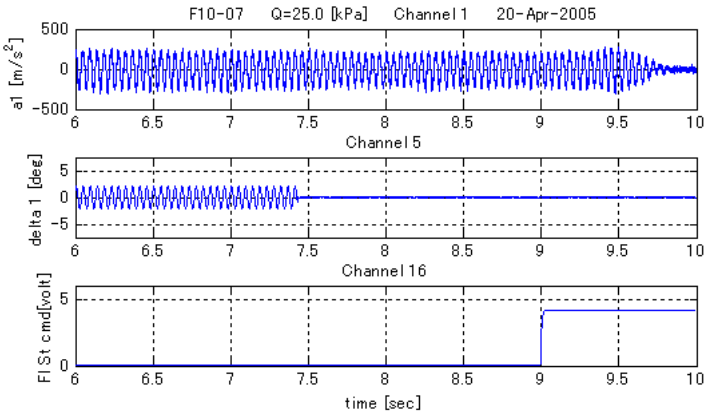

(b) LCO case (4 sec.)

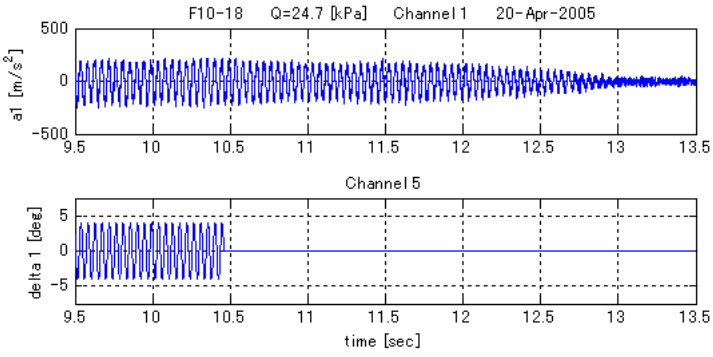

(c) LCO-Stable case (4 sec.)

Fig. 9. Time histories with a time axis enlarged for Fig. 8.

4 New type LCO

In previous tests, once LCO occurred, LCO was kept going even removing excitation. The phenomenon that LCO once occurred goes to rest after removing excitation has not occurred in the previous tests. In this sense, six cases of this type of phenomenon as shown in Fig. 7 from (1) to (6) are new types of LCO observed first in the present test.

Time history data for these six new types of LCO are shown in Fig. 10 where the upper chart shows acceleration a_1 and the lower chart shows l. e. surface deflection δ_1. We can distinguish three different types of LCO among the new types of LCO. The first type occurs in (1) and (2); when stopping oscillation, LCO converges almost at once. The second type is observed in the rest of the cases where we can see such phenomena that oscillation is getting weaker after stopping excitation and finally converging to stop. In case of (5), oscillation with reducing amplitude, sustains for around 10 seconds before converging. For comparison of the new type of the present LCO with the typical LCO, time history charts with a time axis enlarged for 0.5 seconds are shown in Fig. 11. The charts show, from top to bottom, a_1, a_4 and δ_1, where a_1 denotes the output of the inner leading edge accelerometer, a_4 the wing tip trailing edge accelerometer.

Based on these observations, it can be assumed that the present phenomena happened near the saddle-node bifurcation. In Fig. 12 is shown a bifurcation diagram depicted according to the present test results. The vertical axis shows the amplitude of the wing oscillation, while the horizontal axis shows a wind tunnel dynamic pressure. Bifurcation diagram is of subcritical Hopf bifurcation. The vertical line in the figure shows the dynamic pressure at the saddle-node point. Let the dynamic pressure of the wind tunnel change a bit. LCO entered around saddle-node then might come to stable if the dynamic pressure reduces lower than a saddle-node point.

Comparing these time charts, we can observe that fully established LCO in Fig.11 (c) has a simple frequency component even at the wing tip acceleration A4, while in case of new type LCO inFig11 (a) and (b), higher frequency component appears in A4 that might let the wing release from LCO.

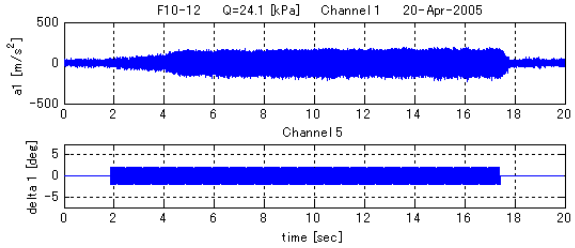

(1) q=24.1 kPa, l.e.=2.0 deg

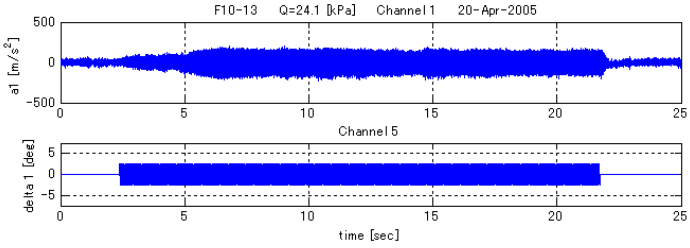

(2) q=24.1 kPa, l.e.=2.5 deg

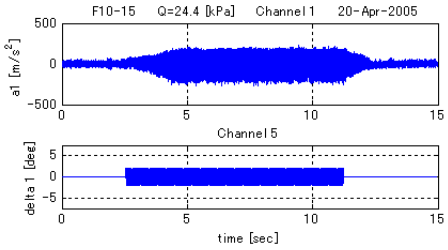

(3) q=24.4 kPa, l.e.=2.0 deg

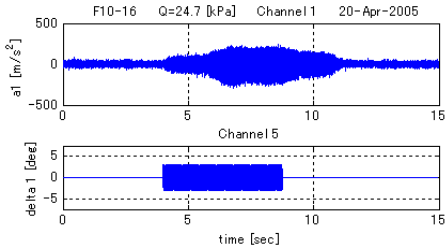

(4) q=24.7 kPa, l.e.=3.0 deg

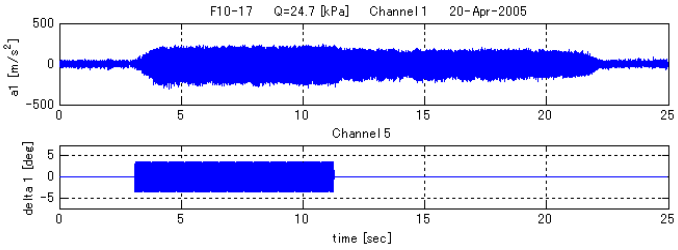

(5) q=24.7 kPa, l.e.=3.5 deg

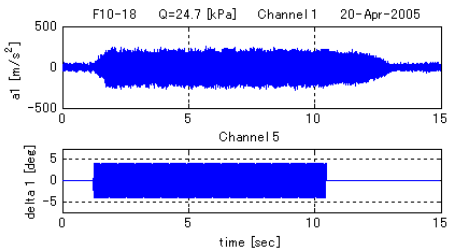

(6) q=24.7 kPa, l.e.=4.0 deg

Fig. 10. Time history of new type LCOs

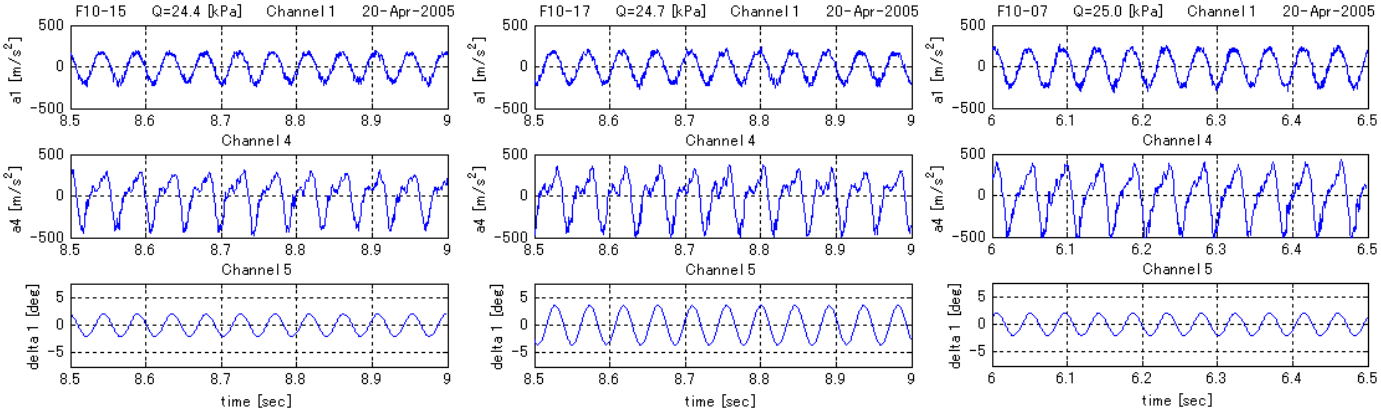

(a) LCO-Stable case
q=24.4 kPa, l.e.=2.0 deg

(b) LCO-Stable case
q=24.7 kPa, l.e.=3.5 deg

(c) LCO case
q=25.0 kPa, l.e.=2.0 deg

Fig. 11. Time histories with a time axis enlarged
for LCO and LCO-Stable case

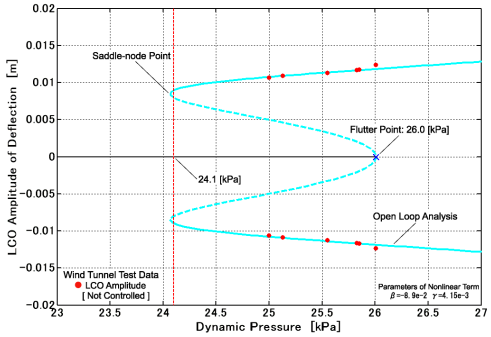

Fig. 12. Bifurcation Diagram

5 Numerical simulation for new type LCO

Based on the assumption stated in the previous chapter, the numerical simulation will confirm that the similar phenomena observed in the test results actually happen. Matsushita et al. have developed a nonlinear mathematical model in the form of 2-DOF, finite state nonlinear differential equation [7]. Introducing the fourth order nonlinearity to the generalized aerodynamic damping terms, they have obtained the following sixth order nonlinear differential equation,

$$\dot{x} = Ax + \Delta Ax + Bu; \quad x = \left[q,\ \dot{q},\ z\right]^T \in R^6 \tag{2}$$

where q is the generalized coordinates and z is the augmented variable expressing the unsteady aerodynamic delay. The matrix A is a linear part of the system matrix and is an ordinary matrix for flutter analysis. It takes a form as,

$$A=\left(a_{ij}\right)=\begin{bmatrix} 0 & I & 0 \\ -(M-A_0)^{-1}(K-A_2) & -(M-A_0)^{-1}(C-A_1) & -(M-A_0)^{-1} \\ B_a & 0 & -\Lambda \end{bmatrix} \in R^{6\times 6}$$

$$B=\begin{bmatrix} 0 \\ -M_q S_\delta K_\delta \\ K_\delta \\ 0 \end{bmatrix} \in R^{141} \tag{3 a, b}$$

In eq. (3), M, C, and K are mass, structural damping, and stiffness matrices, respectively, while A_2, A_1, A_0, B_0 and Λ comprise the finite state aerodynamic model. The matrix ΔA_{NL} in eq. (2) represents a nonlinear terms and has the following form.

$$\Delta A_{NL}=\begin{bmatrix} 0 & 0 & 0 \\ 0 & (M-A_0)^{-1}\Delta A_{1NL} & 0 \\ 0 & 0 & 0 \end{bmatrix} \in R^{6\times 6} \tag{4}$$

$$\Delta A_{1NL}=\begin{bmatrix} (\beta_1 q_1^{\,2}+\gamma_1 q_1^{\,4})a_{11a} & 0 \\ 0 & (\beta_2 q_2^{\,2}+\gamma_2 q_2^{\,4})a_{22a} \end{bmatrix} \tag{5}$$

where a_{11a} and a_{22a} are the aerodynamic damping coefficients for torsion and bending deflection, respectively. The parameters β's and γ's are free parameters to be determined for fitting the wind tunnel test data. Making a lots of efforts to search an optimum combination of parameters, they have reached the bifurcation diagram as shown as a solid line in Fig. 12. The correspondence of the LCO between the math model and the experiment is quite good; the amplitude of LCO is almost identical and the position of the saddle-node bifurcation is exactly the same.

In the present research, the basic nonlinear 2nd order differential equation proposed by Matsushita et al. [8] and shown below that has the same subcritical Hopf bifurcation is used for simulation.

$$\ddot{x} - (\varepsilon - \varepsilon_c + x^2 - 0.5x^4)\dot{x} + x = 0 \tag{6}$$

with ε_c = 1, a bifurcation diagram of this equation has a form shown in Fig. 13 and a saddle-node point lies at (0.75, $\pm\sqrt{2}$).

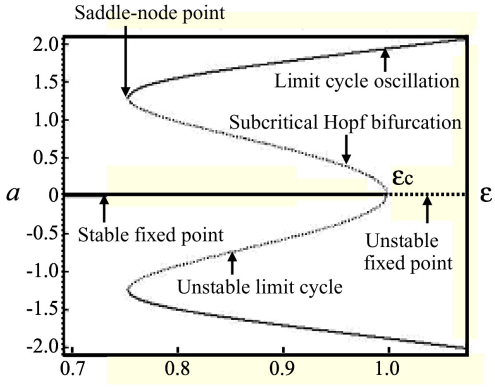

Fig. 13 Bifurcation diagram for eq. (6).

MATLAB Simulink is used for simulation. Forcing function with the frequency 1 Hz of LCO is applied to the right hand side of eq. (5). Amplitude of forcing function is adjusted so as to get the response above the stability boundary. As for the deviation of the dynamic pressure, ε in eq. (6) is varied as a random variable with the intensity (variance) of 0.05.

Fig. 14 shows the simulation results at ε = 0.8 (simulated as dynamic pressure in wind tunnel test) which is a little bit higher than a saddle-node point. Amplitude of forcing is 0.1. In both cases, oscillations are progressing to LCO. Simulation is done at ε = 0.75, near saddle-node point. The results are shown in Fig. 15. Forcing amplitude is set as 0.13. When the control parameter ε is not varied, oscillation is progressing to LCO and keeps oscillating.

However, when ε is varied at random, the phenomena that oscillation is sustained for a while and then converges can be observed. This phenomenon is very much similar to what we observed in the wind tunnel tests as a new type of LCO.

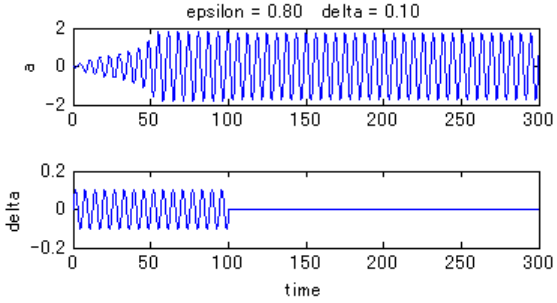

(a) No random variation for ε

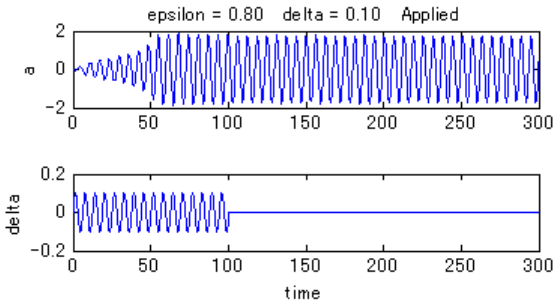

(b) Applied the random variation for ε

Fig. 14. Numerical simulation (ε = 0.8)

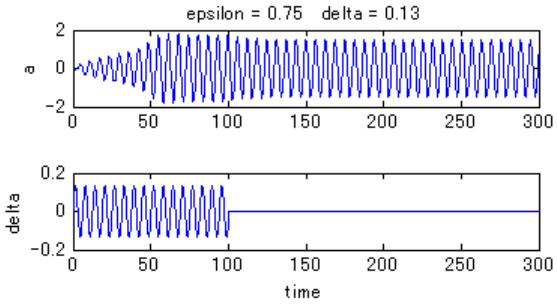

(a). No random variation for ε

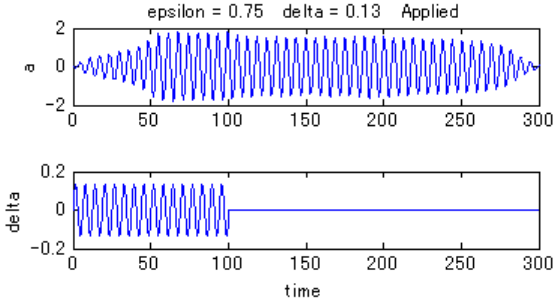

(b) Applied the random variation for ε

Fig. 15. Numerical simulation (ε = 0.75)

6 Conclusions

In the recent transonic wind tunnel test, new type of LCO that LCO once occurred eventually converges to rest after removing excitation was observed. Based on the assumption that the new type of LCO may occur near a saddle-node point, numerical simulation was carried out for a fundamental mathematical model that behaves as a subcritical Hopf bifurcation. The simulation results show qualitatively the same results as in the wind tunnel tests. According to the results, the new type of LCO observed in the recent wind tunnel tests should be happened near a saddle-node bifurcation and the dynamic pressure might be changed a bit.

References

[1] Cunningham A. M. Jr. Practical problem: airplanes. Chapter 3, *Unsteady transonic aerodynamics*, Nixon, D., ed., Progress in Astronautics and Aeronautics, 120, AIAA, pp 75-132, 1989.

[2] Dowell E H. Nonlinear Aeroelasticity. *Flight-Vehicle Materials, Structures and Dynamics*, 5, Part II, Chapter 4, ASME, pp. 213 - 239, 1993.

[3] Schewe G and Deyhle H. Experiments on transonic flutter of a two-dimensional supercritical wing with emphasis on the non-linear effects. *Proceedings of the Royal Aeronautical Society Conference on "UNSTEADY AERODYNAMICS"*, 1996.

[4] Isogai K. On the Transonic-Dip Mechanism of Flutter of a Sweptback Wing, *AIAA Journal*, Vol. 17, No. 7, pp 793-795.

[5] Matsushita H, Miyata T, Christiansen, L E. Lehn-Schioler T and Mosekilde E. On the Nonlinear Dynamics Approach of Modeling the Bifurcation for Transonic Limit Cycle Flutter, *Proceedings of the 24th ICAS*, pp. 414.1-414.8, 2002.

[6] Matsushita H, Saitoh K, and Gránásy P. Nonlinear characteristics of transonic flutter of a high aspect ratio wing. *Proceedings of 21st ICAS*, Melbourne, pp. 1-7, 1998-4.

[7] Matsushita H, Saitoh, K, and Gránásy P. Two degrees-of-freedom nonlinear math model with fourth order nonlinear aerodynamics for transonic limit cycle flutter. *CEAS/AIAA/ICASE/NASA LaRC International Forum on Aeroelasticity and Structural Dynamics 1999*, Williamsburg, US, June 1999.

[8] Matsushita H, Miyata T, Kawai M, and Mosekilde E. Nonlinear Mathematical Modeling of Aircraft Wing Flutter in Transonic Range. *International Conference on Physics and Control*, St. Petersburg, Russia, 2003.